Vapor Nanobubbles around Heated Nanoparticles: Wetting Dependence of the Local Fluid Thermodynamics and Kinetics of Nucleation

Oscar Gutiérrez-Varela, Julien Lombard, Thierry Biben, Ruben Santamaria, Samy Merabia

Wetting dependence of the nucleation kinetics of vapor bubbles around heated nanoparticles.

Oscar Gutiérrez-Varela,[1,2] Julien Lombard,[3] Thierry Biben,[2] Ruben Santamaria,[1] and Samy Merabia[2]

[1] *Instituto de Física, Universidad Nacional Autónoma de México, Ciudad de México, México*

[2] *Univ. Lyon, Université Claude Bernard Lyon 1, CNRS, Institut Lumière Matière, F-69622, Villeurbanne, France*

[3] *Departamento de Física y Química Teórica and Departamento de Matemáticas, Facultad de Química, Universidad Nacional Autónoma de México, Ciudad de México, México*

(Dated: July 17, 2023)

Abstract

Nanoscale boiling is relevant to irradiated plasmonic nanoparticles immersed in water and also to surfaces displaying nanometer scale heterogeneities. Here we show, using molecular dynamics (MD) simulations, that vapor nucleation around heated nanoparticles may be slower in the case of weak water/nanoparticle interactions. This result, which is qualitatively at odd with the predictions of isothermal classical nucleation theory, may be explained by the competition between two antagonist effects : while, classically, hydrophobicity increases the vapor nucleation rate, it also penalizes interfacial thermal transfer, slowing down kinetics. The kinetics of heat transfer from the nanoparticle to water is controlled by the interfacial thermal conductance, which turns out not only to decrease with the nanoparticle hydrophobicity, but also drops down prior to phase change yielding even long nucleation times. Such conclusions have been reached by considering the comparison between MD and continuous heat transfer models. These results put forward the role of the nanoparticle wettability in the generation of plasmonic nanobubbles observed experimentally and open the path to the control of boiling using nanopatterned surfaces. .

I. INTRODUCTION

Boiling, understood as the transition from a liquid state to a vapor state driven by a heated solid surface, may proceed along two different scenarios. Normal boiling occurs when a vapor nucleus is formed and detaches from the solid. For water, this typically corresponds to a local temperature $T_b \sim 373$ K [1]. Explosive boiling occurs either when a fluid is heated up by a solid flat surface in the microscale or when it is heated so fast that it may remain trapped in its metastable state until it crosses the liquid-vapor spinodal line. On ordinary surfaces, normal boiling occurs after gentle heating, while explosive boiling may be reached with high heating rates [2, 3], typically 10^6 K/s [4].

Boiling may be also investigated at the nanoscale. Plasmonic nanoparticles dispersed in water, susceptible to be heated up in a picosecond time scale by a laser, act as local hot spots in the liquid environment and constitute a platform to probe the physics of phase transitions at the nanoscale [5–7]. From a practical perspective, the possibility to convert light into vapor has been exploited in several scientific areas, including nanoparticle assisted cancer therapy [8–10], nano and micro manipulation [11], and photoacoustic imaging [12, 13]. Due to the explosive nature of the generated plasmonic nanobubbles, intense acoustic waves

are emitted, an effect which may be used in the destruction of biological cellular components at the local scale [14–17].

Most of the studies of boiling around hot colloidal nanoparticles are concerned with the temperature threshold to generate vapor nanobubbles, in relation to the fluid spinodal temperature [6, 7, 18–23, 27]. These studies are based on experimental investigations [23–25] or molecular dynamics calculations (MD) using Lennard-Jones models [7, 18–20]. Few studies considered the kinetics of boiling and, in particular, the effect of wetting [19].

In this work, we investigate the effects of wetting on the kinetics of nanoscale boiling. We employ a model of a metallic nanoparticle of tunable wettability immersed in water heated up to high temperatures by a picosecond pulse, and a model of solid surface displaying nanoscale contact angle heterogeneities. Previous simulation works have considered a Lennard-Jones model to describe the fluid [19]. Here, we investigate a nanoparticle immersed in liquid water to go beyond the Lennard-Jones fluid model. We demonstrate that vapor nucleation is faster in the case of strongly hydrophilic nanoparticles, in contrast with the predictions of isothermal classical nucleation theory. In passing, we show that the onset of boiling may be ~ 100 K lower than water spinodal temperature $T_s = 573K$ [1] in the case of weak wetting interactions (contact angle around 70^o). Nanoscale boiling is found to be a relatively slow process whose kinetics is controlled by the time-dependent thermal conductance at the interface between metal and water. This conductance may drop by one order of magnitude depending on wetting, yielding nucleation times much longer than heat diffusion times. All these effects compete to slow down the kinetics of phase change around weakly hydrophilic nanoparticles.

The article has the following structure. In Section 2II, the methodology is presented. In Section 3III, we present the results concerning both the kinetics of nucleation and the thermodynamics of boiling. Finally, in Section 4IV, we present the conclusions of this work.

II. METHODOLOGY

MD simulations are carried out using the free software Large-scale Atomic/Molecular Massively Parallel Simulator (LAMMPS). The nanoparticle consists of a metallic spherical particle immersed in liquid water with fixed diameter of 11 nm, and initially occupies a volume fraction $\Phi \sim 10$ % of the system, as shown in Fig. 1. Periodic boundary condi-

tions are applied in all directions. The metal-metal interactions are described by the Heinz potential [29] while water is described by the flexible TIP4P/2005 [30] model. This model has been chosen because it gives a good description of water coexistence curves [33]. The interaction between the water molecules and the nanoparticle atoms are simulated by a Lennard-Jones (LJ) 12-6 potential. More information on the simulation details are found in the Supplementary material [28].

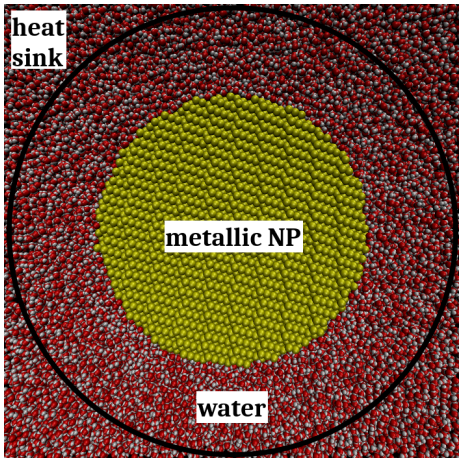

FIG. 1. Representation of the system : a metallic nanoparticle immersed in bulk water.

We consider three different nanoparticle wettabilities: strong, intermediate, and weak wetting. These are defined by the strength of the LJ interactions between the gold and the oxygen atoms through a dimensionless parameter α which enters into the definition of the cross-interaction energy between gold and oxygen atoms $\epsilon_{\mathrm{Au-O}}$:$\epsilon_{\mathrm{Au-O}} = \alpha\epsilon_{AuO}$ with $\epsilon_{AuO} = 0.9898$ Kcal mol^{-1}. The specific values of α for the different wettings considered in this article are: i) strong wetting: $\alpha = 1.0$, ii) intermediate wetting: $\alpha = 0.5$, and iii) weak wetting: $\alpha = 0.3$. The contact angles characterizing the corresponding planar metal/water interfaces, at room temperature, are 20^o, 40^o, and 70^o, respectively. The procedure to measure the contact angles is described in the Supplementary material [28].

The time step of the dynamics is 1 fs. The systems are first thermalized in the NPT ensemble using the Nose-Hoover thermostat-barostat for 300 ps, with a thermostat temperature of 300 K, and a pressure of one atmosphere [31]. After thermalization, isobaric dynamics are carried out in the NPH ensemble (which corresponds to a isoenthalpic-isobaric ensemble, where the number of particles, pressure and enthalpy are fixed) using the Nose-

Hoover barostat.

Mirroring experiments, where a laser pulse heats the nanoparticles, we consider pulses heating the nanoparticle by rescaling the velocities of the metal atoms every 40 ps. The target temperature is fixed at a value between 2000 and 3500 K. Below 2000 K, we observe no boiling of water around the nanoparticle. Note also that after each heat pulse, the nanoparticle relaxes its temperature by redistributing the internal energy in a time < 500 fs. This effective temperature is hundreds of Kelvin less than the temperature to which the nanoparticle was originally heated up by rescaling the atomic velocities. For more details, consult the supplementary material. After each pulse, the temperature of water at a distance greater than 95 Å from the nanoparticle center is set at 300 K just once with the purpose to dissipate heat in the system. Between each temperature rescaling, the system is allowed to relax in the NPH ensemble. We have verified that, for low nanoparticle heating, the steady state temperature profile of water follows the expected $1/r$ behaviour, thus our methodology simulates a semi-infinite system.

III. RESULTS

A. Effect of wetting

Nucleation can be put in evidence by looking at the time evolution of the volume of the system, as represented in Fig. 2. Before nucleation, the volume of the system fluctuates, displaying both positive and negative fluctuations. When a vapor embryo is formed, the volume increases sharply and the last moment where the volume change is negative serves us to define the nucleation time. Strikingly, Fig. 2 shows that the nucleation time increases with the hydrophobicity of the nanoparticle. This observation is in contrast with isothermal classical nucleation theory which predicts a lower energy barrier and higher nucleation rate in the case of weak wetting. To interpret this peculiar kinetics, we will analyze in the following both the local thermodynamics of water at the onset of boiling and the kinetics of heat transfer from the nanoparticle to water.

The generation of a vapor nanobubble is monitored by paying attention at the water density profile, plotted at different times in Fig. 3. Here, we consider that a vapor bubble is formed when the local density is below the water critical density $\rho_c = 322$ kg/m^3 [33].

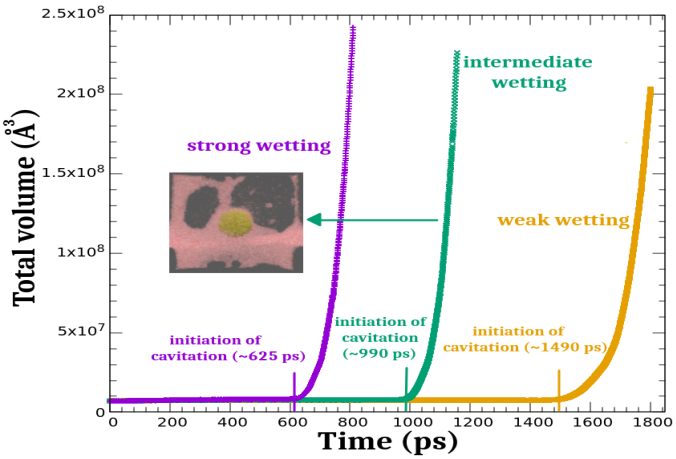

FIG. 2. Evolution of the system volume as a function of time, for different wetting regimes. The nanoparticle heating temperature is 2500 K.

Different scenarios may be encountered depending on the wettability of the nanoparticle. In the case of strong wetting, there is layering of the water molecules in the vicinity of the nanoparticle, which persists when water is heated up by the nanoparticle. As a result of the presence of this layer, the nanobubble is created at a non-vanishing distance $d \simeq 1$ nm from the nanoparticle. This layer is less pronounced in the case of intermediate wetting nanoparticles, and it disappears for weakly wetting nanoparticles. In this latter situation, an appreciable precursor thin vapor layer grows with time, as can be seen in Fig. 4. For weak wetting nanoparticles, the thickness is on the order of 0.7 nm, while it amounts to 0.3 nm in the case of strong wetting. All these observations call for a local thermodynamics analysis of the properties of water in the vicinity $d < 1$ nm of the nanoparticle.

Fig. 5 shows snapshots of the system just before the creation of a vapor nanobubble. It is first worth noting the non-uniform nature of early stage boiling. For time scales of a few tens of picoseconds, nanobubble nucleation around the heated nanoparticle does not occur uniformly. Fig. 5 shows that the formation of a bubble remains spatially localized. The non-uniform nature of boiling is found to be common to all the wetting interactions considered, as presented in the Supplementary Material [28].

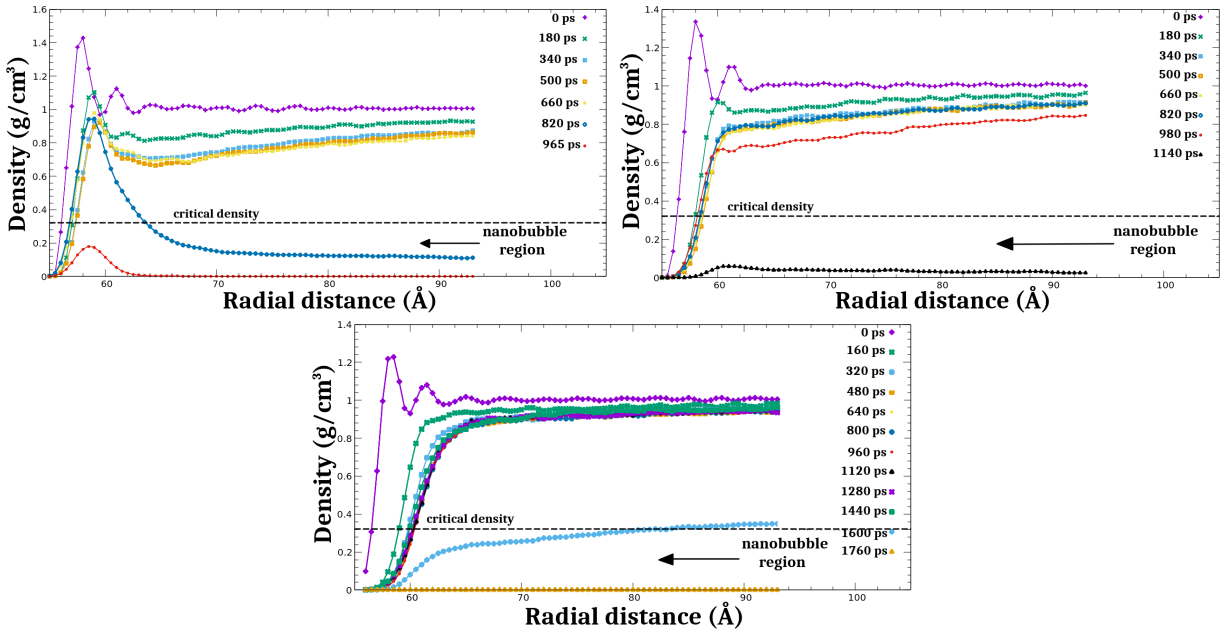

FIG. 3. Density profiles calculated at different times before the generation of a bubble for the different wetting regimes. From top to bottom : strong wetting, intermediate wetting and weak wetting. The nanoparticle heating temperature is 2500 K.

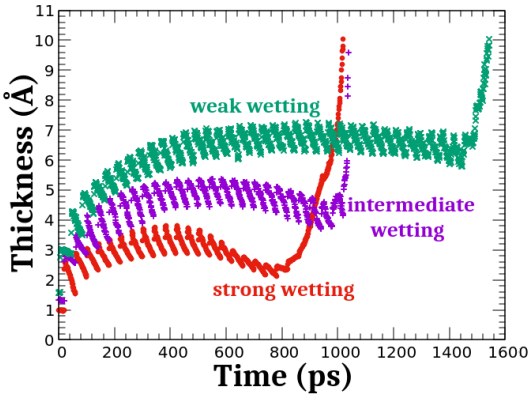

FIG. 4. Evolution of the precursor vapor layer thin film prior to nucleation for different wetting regimes. The nanoparticle heating temperature is 2500 K.

B. Thermodynamics of the fluid in the vicinity of the nanoparticle

We concentrate here on the analysis of the temperature of water in the vicinity of the nanoparticle. In the following, we investigate the temperature at a distance 1 nm from the nanoparticle surface. Such a choice is justified because, first, we already saw in Fig. 3 that

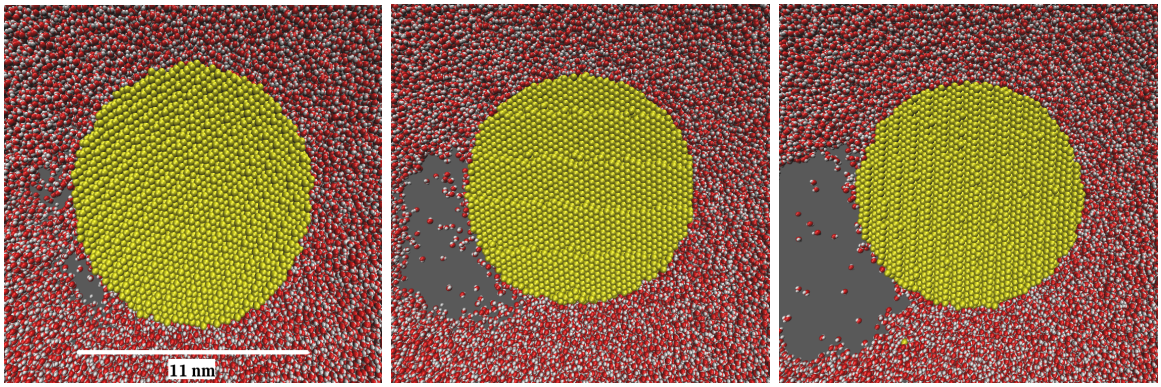

FIG. 5. Snapshots of the early stages of boiling for the strong wetting nanoparticle. The corresponding times are 625, 640, 655 ps respectively, from left to right. The images display ~ 65 % of the simulation box. Snapshots for the intermediate and the weak wetting situations display similar behaviors, as shown in the Supplementary Material [28].

vapor nucleation starts at a finite distance from the nanoparticle. Secondly, we demonstrate in the supplementary material that our conclusions remain qualitatively the same when we deal with distances 0.5 and 1.5 nm from the surface. Finally, previous atomistic simulations showed that spinodal crossing occurs at a distance $0.5 - 1$ nm from the nanoparticle surface [7].

Fig. 6a shows the evolution of the thermodynamic state of water at a distance of 1 nm from the nanoparticle surface. We observe that, locally, water follows the saturation line until its temperature reaches a maximal temperature and a phase change occurs. The maximal temperature reached before phase change depends on the nanoparticle wettability, and is the highest for strong wetting. Fig. 6b shows that the maximal temperature reached by the water surrounding the nanoparticle surface increases linearly with the nanoparticle heating temperature. This behavior is observed for all the wetting regimes, but the temperature reached by water is highest for the strong wetting nanoparticle. From Fig. 6b, one can identify an onset temperature $T_{\mathrm{b}}(\theta)$ which is the minimal temperature to observe boiling. As seen in Fig.6c, this temperature turns out to be a strong function of the contact angle θ that characterizes the wetting between the nanoparticle and water. The weaker the interfacial interaction, the lower the boiling temperature.

The maximal temperature depends on two antagonist effects: the interface thermal resistance between the nanoparticle and water, which is high for weakly wetting interfaces [34–

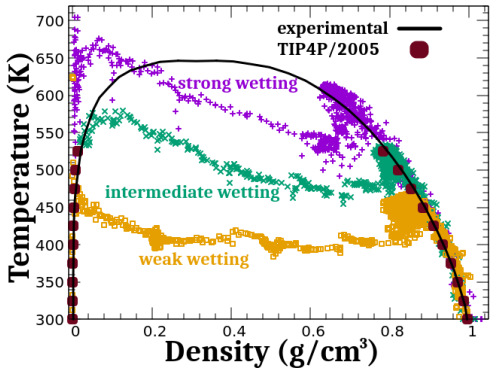

(a)

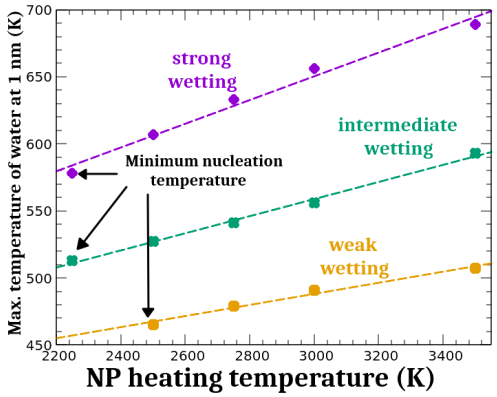

(b)

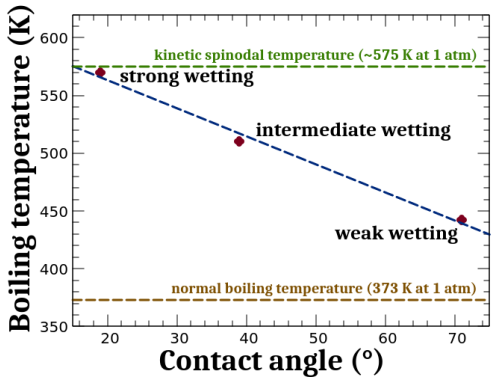

(c)

FIG. 6. a) Evolution of the thermodynamic state of water at $d = 1$ nm from the nanoparticle surface for the nanoparticle heating temperature of 2500 K. b) Maximum temperature reached prior to nucleation by water at 1 nm from the nanoparticle surface as a function of the nanoparticle heating temperature. c) Minimum water temperature, $T_{\mathrm{b}}(\theta)$, needed to observe boiling as a function of the contact angle. This temperature corresponds to water at 1 nm from the nanoparticle surface. The maximal temperatures estimated at distances $d = 0.5$ and 1.5 nm are displayed in the supplementary material [28]. The experimental data are taken from [32] while the TIP4P/2005 model saturation curves are extracted from [33].

36], and the probability to create a vapor bubble which depends on the liquid-solid interface tension and is high for weakly wetting interfaces [37]. The decrease of the boiling temperature with the contact angle that we report demonstrates that the effect of thermal interface resistance dominates over the energy barrier to create a bubble.

In the literature, water spinodal temperature is reported to be $T_s \sim 573$ K [1, 38]. The onset temperature observed in our simulations may be below water spinodal temperature. This contrasts with the general belief that nanobubble generation coincides with the crossing of spinodal temperature [7, 18–23]. Note that the deviations may be large and exceed 100 K for the weak wetting nanoparticle considered here. The strong effect of wetting is also observed when we analyze the temperature of water at distances 0.5 and 1.5 nm from the nanoparticle surface, as shown in the Supplementary material [28].

It is also important to emphasize that the boiling temperatures measured here may be well below the kinetic spinodal temperature of water T_K. The kinetic spinodal temperature, which accounts for the possibility to nucleate vapor by thermal fluctuations of the system, is the effective maximal temperature for which a liquid metastable state can be sustained. From experiments [33, 39–43], we have that T_K varies typically in the range of $560 - 578$ K for water. We also estimated this temperature by employing a free energy model which describes accurately the phase coexistence of water [44] and found that T_K is 18 K below water bulk critical temperature, as detailed in the Supplementary Material [28]. Therefore, the low nucleation temperature that we evidence here are below the water kinetic spinodal temperature.

C. Nucleation kinetics

We turn out to quantify the nanobubble generation kinetics. Fig. 7 displays the nucleation time as a function of the nanoparticle contact angle. This time corresponds to the first instant for which the volume systematically increases, as illustrated in Fig.2. The time to initiate boiling depends on the nanoparticle contact angle. The nucleation time turns out to be longer for large contact angles, a result which contrasts with an isothermal heterogeneous nucleation scenario for which the nucleation energy barrier decreases with the contact angle [46]. The peculiar kinetics outlined here is related to the ability of the heated nanoparticle to transfer energy to its surrounding fluid, as quantified by the interface ther-

mal conductance G_{K} which is represented as a function of time in Fig. 7b. This quantity is measured between each pulse by considering the evolution of the nanoparticle temperature, as shown in Fig. 7c. More precisely, we fit the nanoparticle temperature decay by an exponential function which is found to well describe the MD data between two successive pulses. From the time constant τ of the exponential, we can deduce a value of the thermal conductance using [57]:

$$G_{\mathrm{K}} = \frac{R_{\mathrm{NP}} c_{\mathrm{np}}}{3\tau} \tag{1}$$

where R_{np} and c_{np} are the nanoparticle radius and specific heat capacity per unit volume, respectively. In Fig. 7b, we report the values of the interfacial conductance G_{K} determined in this way every 40 ps. Further details concerning the calculation of the time-dependent interfacial conductance may be found in the Supplementary material [28].

It is also important to remark that boiling is a relatively slow process. The nucleation time measured in MD is at least 10 times larger than the characteristic heat diffusion time over a distance $d = 1$ nm in bulk water, $t_{\mathrm{diff}} = d^2/\alpha_w \sim 10$ ps $<<$ 1 ns, where $\alpha_{\mathrm{w}} = 1.5 \times 10^{-7}$ m^2/s denotes thermal diffusivity of water. Therefore, our results indicate that the phase change phenomenon observed here is not diffusion limited. In the case of low interfacial conductance, an additional relaxation time $\tau_{\mathrm{np}} = c_{\mathrm{np}} R_{\mathrm{np}}/3G_{\mathrm{K}}$ [47] may characterize the nanoparticle cooling. This relaxation time measures the kinetics of the interfacial heat transfer from the nanoparticle to the fluid. In this latter expression, $c_{\mathrm{np}} = 2.5\ 10^6$ J/m^3/K and R_{np} are the specific heat capacity per unit volume and the radius of the nanoparticle, respectively, and G_{K} the gold-water interfacial thermal conductance.

The interfacial conductance G_{K} is found to depend on the contact angle, an effect which has already been investigated [34–36]. In particular, G_{K} decreases with the nanoparticle hydrophobicity, consistently with a slower kinetics of nucleation for weak nanoparticle-water interactions. More surprisingly, the interface conductance significantly decreases with time prior to nucleation, as reported in Fig. 7b. Note that the conductance drop strongly depends on the nanoparticle contact angle, and is more striking for the strong wetting nanoparticle (around 11 fold drop) than for the weakly wetting nanoparticle (2 fold decrease).

Quite generally, the thermal conductance at solid-liquid interfaces depends primarily on the density of the liquid and on the bonding strength of the interface, which is related to the potential energy between the solid and the liquid [58]. Indeed, in the spirit of acoustic mismatch models, a strong bonding at the interface facilitates the transmission of heat between

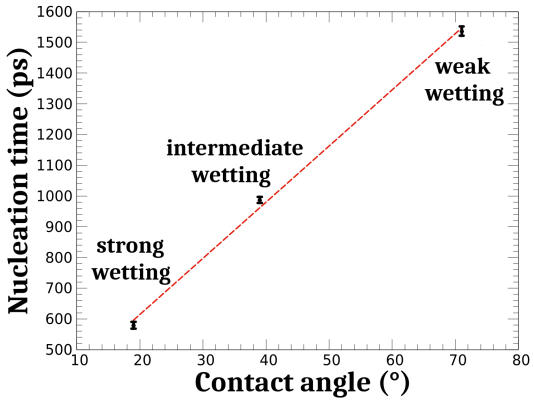

(a)

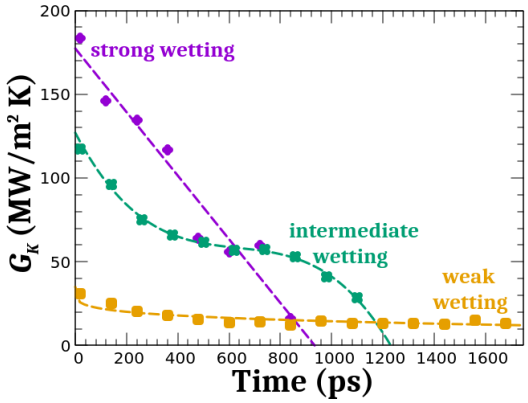

(b)

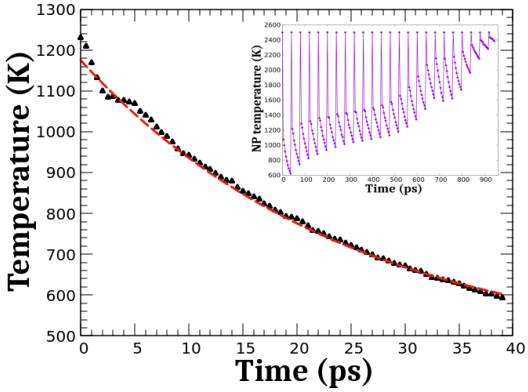

(c)

FIG. 7. a) Nucleation time as a function of the nanoparticle contact angle. Each point corresponds to an average over 10 independent realizations. b) Interfacial thermal conductance G_{K} for the different wetting interactions as a function of the time elapsed prior to boiling. c) Relaxation of the nanoparticle temperature following a heat pulse. The dashed line shows the exponential fit which serves to calculate the interface conductance. The inset shows the nanoparticle temperature during the sequence of heat pulses. The nanoparticle heating temperature is 2500 K.

two media and vice-versa [59]. Note that, for solid-liquid interfaces, a correlation between G_K and the first fluid density peak has been proposed in the literature [60], but we found that such a correlation does not hold in our systems, in line with previous simulations [61].

To interpret physically the decrease with time of the interface thermal conductance G_K, we therefore consider in Fig. 8a, the evolution of the interfacial potential energy as a function of time. Initially, the potential energy is the lowest for the highly hydrophilic nanoparticle, in accordance with the strength of the water-gold interactions. With time, we observe an increase of the potential energy, for all the wetting interactions considered. Eventually, the potential energy vanishes. The increase of the potential energy is related to the decrease of the first density peak as shown in Fig. 8b. The increase of the density is explained by the gradual heating up of the liquid in contact with the nanoparticle. All in all, we see in fig. 8c that the decrease of the interface conductance G_K is strongly correlated with the decrease of the interfacial potential energy. We therefore come to the conclusion that G_K drops with time beause of the gradual decrease of interfacial bonding, an effect which is due to the fluid dilation induced by local heating. The drop is emphasized for strongly hydrophilic nanoparticle, because in this situation the initial interfacial bonding is the largest.

The conductance drop is consistent with the decrease of the cooling rate due to the formation of a vapor layer observed experimentally [5, 48]. As G_K decreases, τ_{np} begins to increase and reaches eventually $\sim$ 500 ps for conductances on the order of $\sim$ 10 MW/(K m^2), which are typical values prior to boiling obtained in this work. The conductance drop is therefore responsible for relatively long cooling times τ_{np} (ns) as Fig.7 gives evidence and thus plays a leading role in the phase change kinetics, as we will confirm by a comparison between MD results and continuum models.

D. Comparison with continuum models

To highlight the role of the time dependent interface conductance, we compare the MD results with the predictions of different continuous models.

In the model denoted Model 1, we take into account the variation of the temperature within the nanoparticle, and the interface conductance between the nanoparticle and water, which is supposed to be constant. The equations are of diffusion type in each medium and are given by:

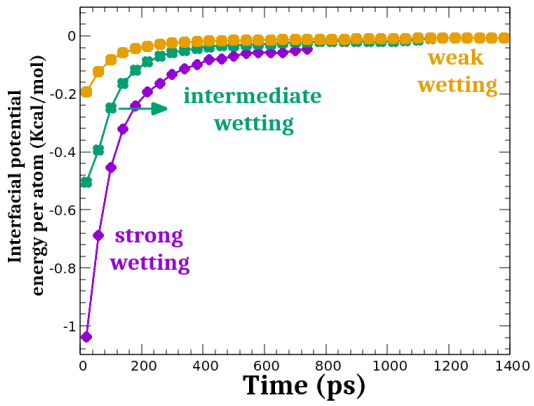

(a)

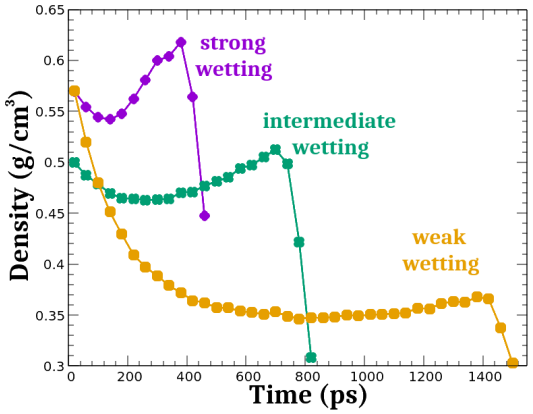

(b)

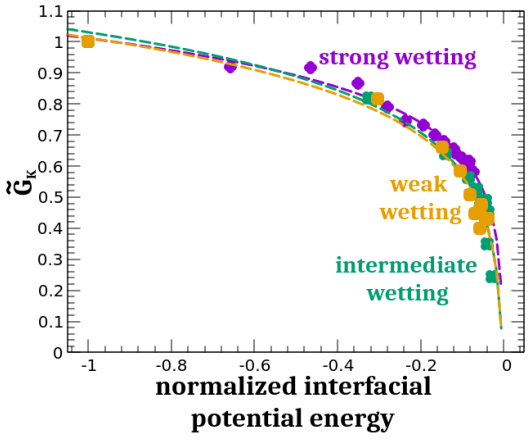

(c)

FIG. 8. a) Evolution of the interfacial potential energy as a function of time for the different wetting regimes. b) Evolution of the local water density with time. The density is averaged over a shell in contact with the nanoparticle and having a thickness 1 nm. c) Normalized interfacial thermal conductance G_K plotted as a function of the normalized interfacial potential energy. Both G_K and the interfacial potential energy have been normalized by their initial values. The nanoparticle heating temperature is 2500 K.

Nanoparticle:

$$\frac{\partial^2(rT_{\rm np})}{\partial r^2} = \frac{r}{\alpha_{\rm np}}\frac{\partial(T_{\rm np})}{\partial t}, \quad \frac{\partial T_{\rm np}(r,t)}{\partial r}|_{r=0} = 0,$$

Nanoparticle-fluid boundary conditions: continuity of the thermal flux

$$-\lambda_{\rm np}\frac{\partial T_{\rm np}(r,t)}{\partial r}|_{r=R_{\rm np}} = G_{\rm k}\left(T_{\rm np}(R_{\rm np},t) - T_{\rm s}(t)\right), \tag{2}$$

Effect of the heating pulse

$$T_{\rm np}(r,0) = T_{\rm np0}$$

Water :

$$\frac{\partial^2(rT_{\rm w})}{\partial r^2} = \frac{r}{\alpha_{\rm w}}\frac{\partial(T_{\rm w})}{\partial t},$$

Continuity of the flux at the nanoparticle-water interface :

$$-\lambda_{\rm w}\frac{\partial T_{\rm w}(r,t)}{\partial r}|_{r=R_{\rm np}} = G_{\rm k}\left(T_{\rm np}(R_{\rm np},t) - T_{\rm s}(t)\right), \tag{3}$$

Boundary condition at infinity :

$$T_{\rm w}(r\to\infty,t) = T_{\rm w0}, \quad T_{\rm s}(0) = T_{\rm w0}.$$

$T_{\rm np}(r,t)$ is the temperature of the nanoparticle at a radial distance r and time t, $\alpha_{\rm np}$ is the thermal diffusivity of the nanoparticle, $R_{\rm np}$ its radius and $\lambda_{\rm np}$ its thermal conductivity. The same definition is used for the water variables and $T_{\rm s}(t) = T_{\rm w}(R_{\rm np},t)$ is water surface temperature. Thermal diffusivity is defined as $\alpha = \lambda/(\rho c_p)$, where λ is the thermal conductivity, ρ is the density, and c_p the specific heat capacity. The value T_{np0} corresponds to the effective temperature after the heat pulse and the subsequent energy redistribution inside the nanoparticle. More information may be found in the Supplementary material. T_{w0} is the initial water temperature, here $T_{w0} = 300$ K.

To solve the coupled Eqs. 2 and 3, a finite difference method is used. To this end, it is necessary to know the values of the thermophysical parameters characterizing the nanoparticle and the surrounding fluid. These values are presented in Table I. The values of the interfacial thermal conductance in the case they are considered constant are the following: *i*) strongly wetting: $G_{\rm K} = 138.175\times10^6$ W/(m^2 K), *ii*) intermediate wetting: $G_{\rm K} = 95.04\times10^6$ W/(m^2 K), and *iii*) weakly wetting: $G_{\rm K} = 59.4\times10^6$ W/(m^2 K). These values were obtained through independent simulations for the systems of this work. In parallel, we also considered the case where $G_{\rm K}\to\infty$.

Parameter	Value	Reference
$\lambda_{\rm np}$	1.7 W/(m K)	[49–51]
$\lambda_{\rm w}$	1.01 W/(K m)	[52]
$c_{\rm p,np}$	129 J/(K kg)	[53]
$c_{\rm p,w}$	4184 J/(K kg)	[54]
$\rho_{\rm np}$	19.3 g/cm^3	[55]
$\rho_{\rm w}$	–	MD data

TABLE I. Parameters used in the different continuum models.

We consider another model for the evolution of the temperature of the nanoparticle, denoted Model 2. This model assumes that the nanoparticle temperature is uniform, however, we take into account the possibility of nanoparticle melting [56]. The evolution equation for the nanoparticle is described by:

$$V_{\rm np}C_{\rm p}\frac{dT_{\rm np}(t)}{dt} = -A_{\rm np}G_k\left(T_{\rm np}(t) - T_s(t)\right) \\ -\Delta H_{\rm f}\frac{H(T_{\rm np}-T_f)}{\tau_f}\exp\left(-\frac{t-t_f}{\tau_f}\right) \tag{4}$$

$V_{\rm np}$ is the nanoparticle volume, $C_{\rm p} = 2.5\times10^6$ J/(m^3 K) is the volumetric heat capacity, $A_{\rm np}$ the surface of the nanoparticle, $\Delta H_{\rm f} = h_m V_{\rm np}$ with $h_m = 1.24\times10^9$ J/m^3 the bulk melting enthalpy of gold, $H(T_{\rm np}-T_{\rm f})$ is the Heaviside step function, and $\tau_f = 30$ ps is the characteristic gold melting time [56]. t_f is the last time when the nanoparticle exceeds the gold melting temperature, which in our case is set to $T_{\rm f} = 1200$ K a value which takes into account the finite nanoparticle size. $T_s(t)$ is the instantaneous surface liquid temperature obtained with Eq. 3.

The last model to be considered is denoted Model 3 and is an extension of Model 2 because it deals with the temporal variation of the interfacial conductance as given in Fig. 7b.

We compare now the predictions of these different models with the molecular dynamics data. Figs. 9a and 9b show that initially the continuum medium models and the MD data quantitatively agree for the strongly wetting and intermediate wetting nanoparticles. Nevertheless, for these two wettings, Model 1 and Model 2 predictions begin to deviate from

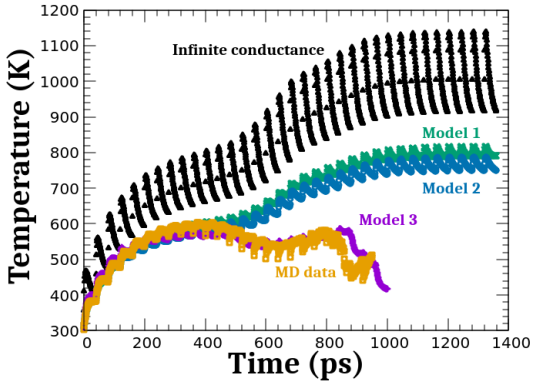

(a) Strong wetting

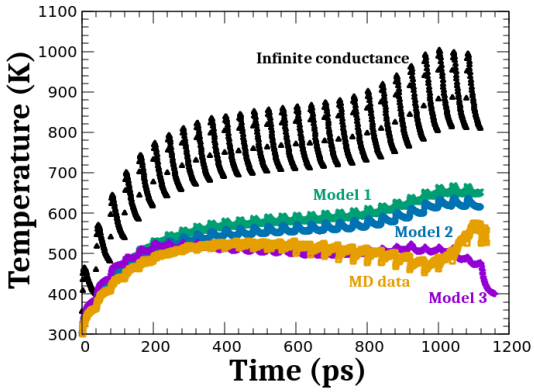

(b) Intermediate wetting

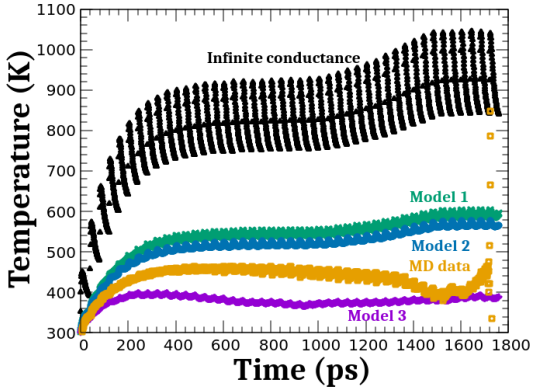

(c) Weak wetting

FIG. 9. Figs. 9a, 9b, and 9c compare the different continuum models and molecular dynamics data for the temperature of water at a distance 1 nm from the surface of the nanoparticle.

the simulation data around time $\sim$ 400 ps. Model 3 describes relatively well all the simulation data for the strongly and intermediate wettings. For the weakly wetting nanoparticle, we

note deviations between the continuum medium models and the simulation data. These relative discrepancies are explained by the existence of a thin layer of low density water that surrounds the nanoparticle, as seen in Fig. 4. In particular, the low density layer is thicker in the weakly wetting case as compared to the strongly and intermediate wettings. The thin vapor layer plays the role of a thermal insulator between the nanoparticle and the liquid water, and should be associated with a local thermal conductivity lower than in the bulk. Heat transport for a weakly wetting interface appears to be more complicated due to the existence of a thin vapor layer, and continuum medium models cannot describe it.

Fig. 10 compares the predictions of the continuous models and the simulation data for the maximal water temperature, as measured 1 nm away from the nanoparticle surface. The highest values of temperature are predicted for the infinite conductance model. Models 1 and 2, which consider a constant conductance, predict also a maximal temperature higher than MD data. Only the model that takes into account the decrease of the thermal conductance with time (Model 3) gives a good account of the simulation data. For the weakly wetting nanoparticle, we note a slight difference between Model 3 predictions and the MD data, but again this should be related to the existence of a thin low density water layer close to the nanoparticle.

Overall, Fig. 10 shows that the kinetics of water heating is controlled by the decrease of the interface conductance with time, and models which ignore this time dependence predict higher maximal temperature, which is faster heating kinetics.

E. Comparison with previous simulation works

A few previous simulation works addressed the phenomenon of nanocavitation around nanoparticles heated by irradiation of laser light, and in this section we discuss some of these studies.

Using nanoparticles immersed in a Lennard-Jones fluid, Sasikumar et al. showed that when considering intense heating of the nanoparticle, the curvature of the interface played an important role in the existence of a nanobubble [18]. They found that for small nanoparticles, the liquid surrounding the surface can maintain temperatures above boiling point without a liquid-vapor phase transition. They even reported that for nanoparticles with a radius smaller than 2 nm, steam generation is not observed even when the fluid is heated up above

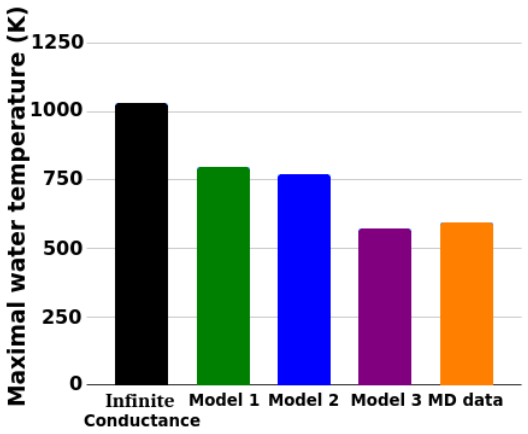

(a) Strong wetting

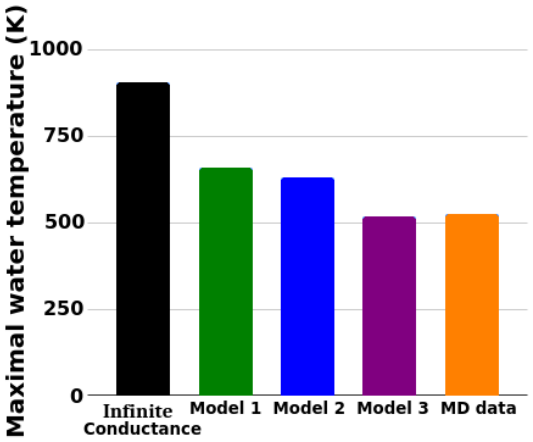

(b) Intermediate wetting

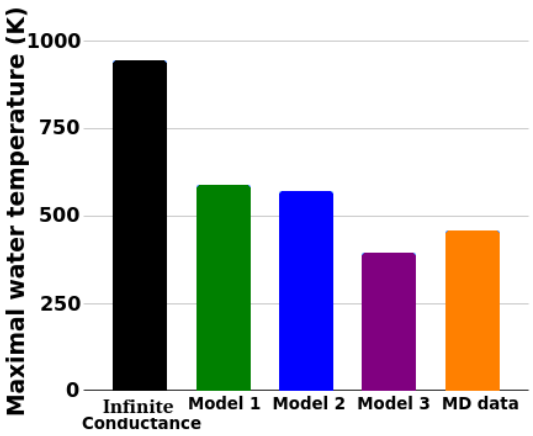

(c) Weak wetting

FIG. 10. Comparison between the Molecular Dynamics data and the different continuum-medium models for the maximum water temperature at a distance 1 nm from the nanoparticle surface.

its critical temperature. They associated the behavior of the fluid close to the interface to the existence of high pressures induced by the surface curvature (Laplace's equation), which suppresses liquid-vapor phase transition. In another work, by considering a similar system, Sasikumar et al. studied the dynamics of the bubbles generated around heated nanoparticles [7]. They observed that for a 8 nm diameter nanoparticle, bubble formation begins when a 1 nm thick liquid layer surrounding the nanoparticle reaches a temperature, close to the bulk spinodal temperature of $0.9T_c$, with T_c the critical temperature. For this reason, they interpreted the formation of bubbles around heated nanoparticles as a spinodal process.

Also, we can deduce from previous works that the evolution of the nanobubble may depend upon the way in which the nanoparticle is heated up. Pu et al. used solid nanoparticles with two different wettabilities immersed in a Lennard-Jones fluid, and they were heating up the nanoparticles slowly until they reached melting temperature [19]. The authors of this work put a constant heating energy that is deposited continuously in the nanoparticle. They observe that for a superhydrophobic (weak wetting) nanoparticle, the radius of the nanobubble grows continuously and slowly until it reaches a maximum value of 10 Å, but this does not occur in an explosive way. They also observed that for a superhydrophilic (super strong wetting) nanoparticle, after a certain time, a bubble appeared with a rapid growth and then had a slow growth until reaching a radius close to 20 Å. In this case, they never observed an explosive growth of the volume of the system.

In the present work, an explosive nanocavitation is observed regardless of wetting, the only thing that is different is the time to reach nanocavitation. It could be that the authors of the previously mentioned work are in the vapor layer growth regime discussed in a previous subsection, and they never reach an explosive nanocavitation because energy is deposited in the nanoparticle in a very slow way. In contrast, in the present work, a large amount of energy bringing the nanoparticle to high temperatures is deposited frequently. These differences in the ways the nanoparticle is heated up could establish methodologies to realize either a vapor layer or an explosive nanocavitation.

IV. CONCLUSION

Using molecular dynamics simulations, we model experiments in which plasmonic nanoparticles dispersed in an aqueous medium are heated by means of strong ultra-short pulsed

lasers. Of particular interest, here, is the effect of the nanoparticle wettability on the dynamics of nanobubble generation, which occurs under situations of strong heating.

We show that nanobubbles may nucleate faster on hydrophilic nanoparticles, a result in contrast with isothermal classical nucleation theory. This kinetics may be explained by the competition between two antagonist effects : on the one hand, the thermodynamics of boiling, and on the other hand, the kinetics of heat transfer from the nanoparticle to water.

We saw that the thermodynamics of boiling may be characterized by an onset temperature which decreases with the hydrophobicity of the nanoparticle. In passing, we noted that locally the onset temperature may be well below water spinodal temperature $\sim$ 573 K. Therefore, the generation of nanobubbles does not necessarily coincide with the crossing of the spinodal line, as commonly assumed in the literature.

Nanoscale boiling kinetics is controlled by the solid/water interfacial thermal conductance, which determines the rate of heat exchange between the nanoparticle and water. The interface thermal conductance is found to decrease with the hydrophobicity of the nanoparticle, but importantly depends also on time. This time dependence may be related to the gradual formation of a low density layer in contact with the nanoparticle, which hinders interfacial heat transfer. The comparison between the atomistic simulations and the predictions of continuum models allows us to explain quantitatively the peculiar kinetics of vapor embryo generation. From this analysis, we found that the interface thermal conductance, and its variation with wetting and time, plays the leading role in the nanobubble generation kinetics. In particular, long nucleation times observed for weakly hydrophilic nanoparticles are explained by the relatively low interface thermal conductance, despite lower boiling temperatures.

Beyond spherical nanoparticles, it remains a future direction of research to investigate boiling close to composite surfaces displaying nanometer scale heterogeneities. Considering nanoscale patches with different contact angles is a promising strategy to tune the boiling properties of solid surfaces.

ACKNOWLEDGMENT

We acknowledge fruitful discussions with F. Caupin, X. Noblin, M. Orrit and Y. Yamaguchi. All the simulations were run at the PSMN (Pôle de Scientifique de Modélisation

Numérique) of the ENS Lyon. Funding from the IDEX Lyon program, the Van Gogh PHC project nanocalefaction, and the ANR project CASTEX are acknowledged.

[1] A. Vogel and V. Venugopalan, Mechanisms of pulsed laser ablation of biological tissues; Chem. Rev. **103** 577 (2003).

[2] J. E. Sheperd and B. Strutevand, Rapid evaporation at the superheat limit; J. Fluid. Mech. **121** 379 (1982)

[3] V. P. Skirpov, Metastable Liquids, Wiley, New-York (1974).

[4] A. Miotello and R. Kelly, Laser-induced phase explosion: new physical problems when a condensed phase approaches the thermodynamic critical temperature", Appl. Phys. A **69** S67-S73 (1999)

[5] V. Kotaidis, C. Dahmen, G. von Plessen, F. Springer, and A. Plech, Excitation of nanoscale vapor bubbles at the surface of gold nanoparticles in water; Journal of Chemical Physics **124**; 184702 (2006).

[6] Y. Wang, M. E. Zaytsev, G. Lajoinie, H. L. The, J. C. T. Eijkel, et al.; Giant and explosive plasmonic bubbles by delayed nucleation; Proceedings of the National Academy of Sciences **115** (30); pp. 7676-7681 (2018).

[7] K. Sasikumar and P. Keblinski; Molecular dynamics investigation of nanoscale cavitation dynamics; The Journal of Chemical Physics **141** (23); 234508 (2014).

[8] J. Shao, M. Xuan, L. Dai, T. Si, J. Li, and Q. He; Near-Infrared-Activated Nanocalorifiers in Microcapsules: Vapor Bubble Generation for In Vivo Enhanced Cancer Therapy; Angewandte Chemie International Edition **54** (43); pp. 12782-12787 (2015).

[9] C. M. Pitsillides, E. K. Joe, X. Wei, R. R. Anderson, and C. P. Lin; Selective cell targeting with light-absorbing microparticles and nanoparticles; Biophysical Journal **84** (6); pp. 4023–4032 (2003).

[10] M. Kitz, S. Preisser, A. Wetterwald, M. Jaeger, G.N. Thalmann and M. Frenz; Vapor bubble generation around gold nanoparticles and its application to damaging of cells; Biophys. Opt. Exp. **2** (2011) 291.

[11] C. Zhao, Y. Xie, Z. Mao, Y. Zhao, J. Rufo, S. Yang, T. J. Huang, et al.; Theory and experiment on particle trapping and manipulation via optothermally generated bubbles; Lab Chip **14** (2); pp. 384–391 (2014).

[12] D. Lapotko; Plasmonic nanoparticle-generated photothermal bubbles and their biomedical applications; Nanomedicine **4** (7); pp. 813–845 (2009).

[13] V. P. Zharov; Ultrasharp nonlinear photothermal and photoacoustic resonances and holes beyond the spectral limit; Nature Photonics **5** (2); pp. 110–116 (2011).

[14] C. P. Lin and M. W. Kelly, Cavitation and acoustic emission around laser-heated microparticles, **72** 2800 (1998)

[15] E. Faraggi, B.S. Gerstman and J. Sun, Biophysical effects of pulsed lasers in the retina and other tissues containing strongly absorbing particles: shockwave and explosive bubble generation, J. Biomed. Opt., **10** (2005) 064029

[16] D. Wen, Intracellular hyperthermia: nanobubbles and their biomedical applications, Int. J. hyperthermia **25** 533 (2009).

[17] J. Lombard, J. Lam, F. Detcheverry, T. Biben, and S. Merabia; Strong and fast rising pressure waves emitted by plasmonic vapor nanobubbles; Phys. Rev. Res., **3** 023231 (2021).

[18] K. Sasikumar, Z. Liang, D. G. Cahill, and P. Keblinski; Curvature induced phase stability of an intensely heated liquid; The Journal of Chemical Physics **140** (23); 234506 (2014).

[19] J. H. Pu, J. Sun, W. Wang, and H. S. Wang; Generation and Evolution of Nanobubbles on Heated Nanoparticles: A Molecular Dynamics Study; Langmuir; (2020).

[20] S. Maheshwari, M. van der Hoef, A. Prosperetti and D. Lohse, Dynamics of formation of a vapor nanobubble around a heated nanoparticle, J. Phys. Chem. C (2018) **122** 20571.

[21] H. Loewen and P. Madden, A microscopic mechanism for shock-wave generation in pulsed-laser-heated colloidal suspensions, J. Chem. Phys. **97** (1992)

[22] F. Caupin and E. Herbert, Cavitation in water : a review, C.R. Physique, **7** (2006) 1000

[23] L. Hou, M. Yorulmaz, N. R. Verhart, and M. Orrit; Explosive formation and dynamics of vapor nanobubbles around a continuously heated gold nanosphere; New Journal of Physics **17** (1); 013050 (2015).

[24] A. Siems, S. A. L. Weber, J. Boneberg and A. Plech, Thermodynamics of nanosecond nanobubble formation at laser-excited metal nanoparticles, New Jour. Phys., **13** 043018 (2011)

[25] M.T. Carlson, A.J. Green and H.H. Richardson, Superheating water by CW excitation of gold nanodots, Nanoletters, **12** 1534 (2012)

[26] G. Baffou, J. Polleux, H. Rigneault and S. Monneret, Super-heating and micro-bubble generation around plasmonic nanoparticles under cw illumination ,J. Phys. Chem. C (2014) **118**

4890-4898

[27] A.A. Alaulamie, S. Baral, S.C. Johnson and H.H. Richardson, Targeted nanoparticle thermometry : a method to measure local temperature at the nanoscale point where water vapor nucleation occurs, Small **13** (2016)

[28] See Supplementary Material Ref

[29] H. Heinz, R. A. Vaia, B. L. Farmer, and R. R. Naik; Accurate Simulation of Surfaces and Interfaces of Face-Centered Cubic Metals Using 12-6 and 9-6 Lennard-Jones Potentials; The Journal of Physical Chemistry C 112 (44); pp. 17281-17290 (2008).

[30] J. L. F. Abascal and C. Vega; A general purpose model for the condensed phases of water: TIP4P/2005; The Journal of Chemical Physics **123** (23); 234505 (2005).

[31] R. Santamaria and J. Soullard; Revisiting particle dynamics in the NPT ensemble under the extended Lagrangian approach; Molecular Simulations; Accepted Manuscript; 2023.

[32] C. Vega, J. L. F. Abascal, and I. Nezbeda; Vapor-liquid equilibria from the triple point up to the critical point for the new generation of TIP4P-like models: TIP4P/Ew, TIP4P/2005, andTIP4P/ice; The Journal of Chemical Physics **125** (3); 034503 (2006).

[33] Material Measurement Laboratory. (2018). SAT-TMMC: Liquid-Vapor coexistence properties - TIP4P/2005 Water (LRC). May 2021, from National Institute of Standars and Technology, Web site: https://www.nist.gov/mml/csd/chemical-informatics-research-group/sat-tmmc-liquid-vapor-coexistence-properties-tip4p2005.

[34] Z. Ge, D. Cahill, and P. Braun; Thermal conductance of hydrophilic and hydrophobic interfaces, *Phys. Rev. Lett.* **96** (2006) 186101

[35] N. Shenogina, R. Godawat, P. Keblinski, and S. Garde; How wetting and adhesion affect thermal conductance of a range of hydrophobic to hydrophilic aqueous interfaces, *Phys. Rev. Lett.* **102** (2009) 156101

[36] A. S. Tascini, J. Armstrong, E. Chiavazzo, M. Fasano, P. Asinari, and F. Bresme; Thermal transport across nanoparticle-fluid interfaces: the interplay of interfacial curvature and nanoparticle-fluid interactions; Physical Chemistry Chemical Physics **19** (4); pp. 3244–3253; 2017.

[37] V. P. Carey; Liquid-vapor phase change phenomena, Taylor and Francis Group, New-York.

[38] R. Thiery, S. Loock, and L. Mercury; Explosive properties of superheated aqueous solutions in volcanic and hydrothermal systems; Metastable Systems under Pressure, Springer; pp.

293–310; 2010.

[39] E. Trinh and R. E. Apflel, J. Chem. Phys. **69** (1978) 4245.

[40] V. N. Estefeev, V. N. Chukanov and V. P. Skirpov, High Temp. **15** (1977) 550

[41] V. N. Estefeev, V. P. Skirpov and V. P. Chukanov, High Temp. **17** (1979) 252

[42] Q. Zheng, D.J. Durben, G.H. Wolf and C.A. Angell, Liquids at large negative pressures: water at the homogeneous nucleation limit, Science, **254** 829-832 (1991).

[43] S.B. Kiselev, Physica A **269** (1999) 252-268.

[44] C. A. Jeffery and P. H. Austin, A new analytical equation of state for liquid water, J. Chem. Phys, **110** 484 (1999).

[45] V. Gerweck and G. Yadigaroglu; A local equation of state for a fluid in the presence of a wall and its application to rewetting; International Journal of Heat and Mass Transfer **35**; pp. 1823–1832; 1992.

[46] M. Pellegrin, Y. Bouret, F. Celestini and X. Noblin, Cavitation mean expectation time in a stretched Lennard-Jones fluid under confinement, *Langmuir* **36** (2020) 14181

[47] G. Baffou and H. Rigneault; Femtosecond-pulsed optical heating of gold nanoparticles; Physical Review B **84**; 035415; (2011).

[48] T. Jollans and M. Orrit; Explosive, oscillatory and Leidenfrost boiling at the nanoscale; Physical Review E **99**; 063110 (2019).

[49] X. Chen, A. Munjiza, K. Zhang, and D. Wen; Molecular Dynamics Simulation of Heat Transfer from a Gold Nanoparticle to a Water Pool; The Journal of Physical Chemistry **C 118** (2); pp. 1285-1293 (2014).

[50] C. F. Richardson and P. Clancy; Contribution of thermal conductivity to the crystal-regrowth velocity of embedded-atom-method-modeled metals and metal alloys; Physical Review B **45** (21); pp. 12260–12268 (1992).

[51] S. Kuang and J. D. Gezelter; A gentler approach to RNEMD: Nonisotropic velocity scaling for computing thermal conductivity and shear viscosity; The Journal of Chemical Physics **133** (16); 164101 (2010).

[52] Römer, F., Lervik, A., and Bresme, F.; Nonequilibrium molecular dynamics simulations of the thermal conductivity of water: A systematic investigation of the SPC/E and TIP4P/2005 models; The Journal of Chemical Physics **137** (7); (2012).

[53] D. Werner, S. Hashimoto, and T. Uwada; Remarkable Photothermal Effect of Interband Excitation on Nanosecond Laser-Induced Reshaping and Size Reduction of Pseudospherical Gold Nanoparticles in Aqueous Solution; Langmuir **26** (12); pp. 9956–9963 (2010).

[54] Open University (2008). S104 Book 3 Energy and Light, p. 59. The Open University.

[55] Charles E. Ophartd. (2003). Density of Gold. May 2021, from Elmhurst College Web site: http://chemistry.elmhurst.edu/vchembook/125Adensitygold.html

[56] J. Lombard, T. Biben, and S. Merabia; Threshold for Vapor Nanobubble Generation Around Plasmonic Nanoparticles; The Journal of Physical Chemistry C **121** (28); pp. 15402-15415 (2017).

[57] A. Rajabpour, R. Seif, S. Arabha, M. M. Heyhat, S. Merabia and A. Hassanali; Thermal transport at a nanoparticle-water interface: a molecular dynamics and continuum modeling study; The Journal of Chemical Physics **150** 114701 (2019)

[58] S. Merabia, J. Lombard, and A. Alkurdi; Importance of viscoelastic and interface bonding effects in the thermal boundary conductance of solid-water interfaces; International Journal of Heat and Mass Transfer **100**; pp. 287–294; 2016.

[59] R. Prasher; Acoustic mismatch model for thermal contact resistance of van der Waals contacts; Applied Physics Letters **94**; 041905; 2009.

[60] D. Alexeev, J. Chen, J. H. Walther, P. Konstantinos, P. Angelikopoulos, and P. Koumoutsakos; Kapitza Resistance between Few-Layer Graphene and Water: Liquid Layering Effects; Nano Letters **15** (9); pp. 5744–5749; 2015.

[61] O. Gutiérrez-Varela and S. Merabia, and R. Santamaria; Size-dependent effects of the thermal transport at gold-nanoparticle-water interfaces; J. Chem. Phys. **157**; 084702; 2022.